Chapter 10
Analytical Approach to a Two-Module Vibro-Impact System

Pawel Fritzkowski, Roman Starosta and Jan Awrejcewicz

Abstract A mechanical system composed of two weakly coupled vibro-impact modules under harmonic excitation is considered. The mathematical model of the system is presented in a non-dimensional form. The analytical approach based on the combination of the multiple scales method and the saw-tooth function is employed. The periodic responses of the system with two impacts per cycle near 1:1 resonance are studied. The results have semi-analytical character. Stability of the periodic motions is evaluated. In the unstable case, occurrence of a different response regime is shown: the strongly modulated response. The analytical predictions are compared with purely numerical results.

10.1 Introduction

Vibro-impact processes arise in many areas of physical science and engineering. Computational analysis and understanding of the mechanical systems in which systematic collisions occur requires specific approaches and tools. From the theoretical point of view, the vibro-impact systems, even the simplest ones, are strongly nonlinear. Their non-smooth dynamics and complex behaviours make it practically impossible to formulate general analytical solutions or strategies.

Many approximate analytical methods suitable for nonlinear dynamical systems have evolved from the classical perturbation approach. Therefore, their applicability is usually limited to weakly nonlinear problems [1, 2]. However, over past decades,

P. Fritzkowski (✉) · R. Starosta
Institute of Applied Mechanics, Poznan University of Technology,
ul. Jana Pawła II 24, 60-965 Poznań, Poland
e-mail: pawel.fritzkowski@put.poznan.pl

J. Awrejcewicz
Department of Automatics and Biomechanics, Technical University of Łódź,
ul. Stefanowskiego 1/15, 90-924 Łódź, Poland

M. Belhaq (ed.), *Topics in Nonlinear Mechanics and Physics*,
Springer Proceedings in Physics 228, https://doi.org/10.1007/978-981-13-9463-8_10

a number of analytical techniques have been developed to cope with vibro-impact models, e.g. the power-law phenomenological modeling [3], the Ivanov non-smooth coordinate transformation [3], the non-smooth temporal transformation (NSTT) [3–5], the concept of impact modes [6].

In particular, a combination of the multiple scales method with a saw-tooth function has been recently applied to the systems including vibro-impact nonlinear energy sink (VI NES) [7–12]. Such problems are strictly connected with the increasingly extensive studies on targeted energy transfer (TET) and energy harvesting [13]. However, this analytical approach has been used to relatively simple systems (two degrees of freedom: one primary oscillator and one impacting particle).

In what follows, a more complicated mechanical system is considered. It consists of two weakly coupled vibro-impact modules under harmonic forces. The main aim of this chapter is to present the applicability of the abovementioned method to the four-degree-of-freedom system. The response of the system in the case of 1:1 resonance is studied, and the effect of selected model parameters on the dynamics is analyzed.

10.2 Mechanical System and Mathematical Model

Consider a two-module system schematically illustrated in Fig. 10.1. Each module consists of two interacting parts: a primary body (box) of mass M, and a particle of mass m, moving freely in a straight cavity. Basically, the boxes themselves are linear oscillators (LO) with viscous damping and harmonic excitation. The stiffness constants of linear springs and the damping coefficients are denoted by k_i and c_i, respectively ($i = 1, 2$). The external forces, in turn, take the form $F_i(t) = F_{i0}\sin(\omega_i t)$. The modules are interconnected by a linear spring and damper (k_{12} and c_{12}).

Mass of the balls is assumed to be relatively small ($M \ll m$). Impacts between the particles and the boxes are characterized by the restitution coefficient, κ. We focus on the case of imperfectly elastic collisions ($0 < \kappa < 1$). Moreover, the coupling between the two modules is supposed to be weak ($k_{12} \ll k_1,\ k_2$ and $c_{12} \ll c_1,\ c_2$). Friction and any other resistance forces in the system are neglected.

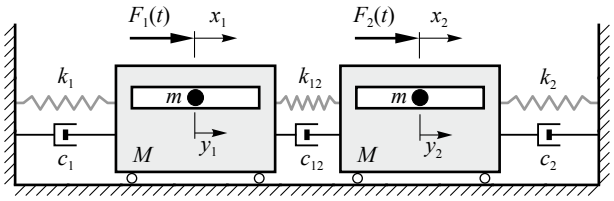

Fig. 10.1 The vibro-impact system to be considered

A single-module system of this type was analyzed by Gendelman [7] as well as Gendelman and Alloni [8]. The analytical approach proposed in these papers has been adpoted and used in our studies.

In recent years, different configurations of primary structures and NESs have been investigated analytically, numerically as well experimentally, and the researches are not of a purely theoretical nature. Particularly, VI NESs are simple in construction and have been found to be very efficient devices with the capacity for rapid energy absorption. Thus, they can be used to suppress shock effects, e.g. in structures under seismic vibrations or in vehicles during collisions [13]. The presented studies, focused on various response regimes and stability of analytical solutions, are the first step, and can be followed by optimization of the VI NES to obtain the most efficient response regime.

Let x_i and y_i denote the absolute displacements of the primary bodies and the balls ($-L \leqslant y_i \leqslant L$, see Fig. 10.2). Using these variables as the generalized coordinates, we can write the equations of motion of the four-degree-of-freedom system between impacts (for $|x_i - y_i| < L$) as:

$$\begin{aligned} &M\ddot{x}_1 + c_1\dot{x}_1 + k_1x_1 - c_{12}(\dot{x}_2 - \dot{x}_1) - k_{12}(x_2 - x_1) = F_{10}\sin(\omega_1 t) \\ &m\ddot{y}_1 = 0 \\ &M\ddot{x}_2 + c_2\dot{x}_2 + k_2x_2 + c_{12}(\dot{x}_2 - \dot{x}_1) + k_{12}(x_2 - x_1) = F_{20}\sin(\omega_2 t) \\ &m\ddot{y}_2 = 0 \end{aligned} \tag{10.1}$$

We assume that the duration of the box-ball collision is very short, and the classical approach can be applied: the simplest impact law (Newton's restitution rule) together with the law of conservation of linear momentum [14, 15].

Let us introduce the dimensionless time and displacements:

$$\tau = \omega_{10}t, \qquad \omega_{10}^2 = \frac{k_1}{M}, \qquad X_i = \frac{x_i}{L}, \qquad Y_i = \frac{y_i}{L}$$

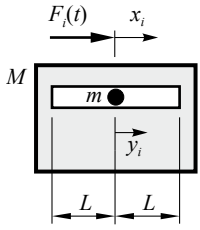

Fig. 10.2 A single module of the system and the characteristic dimension

Taking into account the mentioned standard description of impacts, equations of motion (10.1) can be reformulated and written in the non-dimensional form:

$$\begin{aligned}
&\ddot{X}_1 + \gamma_1 \dot{X}_1 + X_1 - \gamma_{12}(\dot{X}_2 - \dot{X}_1) - \alpha_{12}(X_2 - X_1) = \\
&\qquad = -\varepsilon \frac{1+\kappa}{1+\varepsilon} \sum_j (\dot{X}_1^- - \dot{Y}_1^-)\delta(\tau - \tau_j) + f_{10}\sin(\Omega_1 \tau) \\
&\qquad \varepsilon \ddot{Y}_1 = \varepsilon \frac{1+\kappa}{1+\varepsilon} \sum_j (\dot{X}_1^- - \dot{Y}_1^-)\delta(\tau - \tau_j) \\
&\ddot{X}_2 + \gamma_2 \dot{X}_2 + \Omega_{20}^2 X_2 + \gamma_{12}(\dot{X}_2 - \dot{X}_1) + \alpha_{12}(X_2 - X_1) = \\
&\qquad = -\varepsilon \frac{1+\kappa}{1+\varepsilon} \sum_j (\dot{X}_2^- - \dot{Y}_2^-)\delta(\tau - \tau_j) + f_{20}\sin(\Omega_2 \tau) \\
&\qquad \varepsilon \ddot{Y}_2 = \varepsilon \frac{1+\kappa}{1+\varepsilon} \sum_j (\dot{X}_2^- - \dot{Y}_2^-)\delta(\tau - \tau_j)
\end{aligned} \tag{10.2}$$

where

$$\varepsilon = \frac{m}{M}, \quad \Omega_{20}^2 = \frac{k_2}{M\omega_{10}^2}, \quad \gamma_1 = \frac{c_1}{M\omega_{10}}, \quad \gamma_2 = \frac{c_2}{M\omega_{10}},$$

$$\alpha_{12} = \frac{k_{12}}{M\omega_{10}^2}, \quad \gamma_{12} = \frac{c_{12}}{M\omega_{10}}, \quad \Omega_i = \frac{\omega_i}{\omega_{10}}, \quad f_{i0} = \frac{F_{i0}}{ML\omega_{10}^2}.$$

Obviously, now the overdots denote differentiation with respect to τ. Moreover, $\delta(\bullet)$ stands for the Dirac delta function, τ_j is the time instance of the jth impact (for $|X_i - Y_i| = 1$), and $\dot{X}_i^-$, $\dot{Y}_i^-$ are the velocities immediately before the impact. The sums on the right-hand sides of (10.2) come just from the simple impact model and correspond to the momenta transferred to/from the primary oscillators in consecutive impacts (e.g. see [7, 8]).

For the convenience of further analytical studies, the following new coordinates are defined:

$$U_i = X_i + \varepsilon Y_i, \qquad W_i = X_i - Y_i \qquad (i = 1,\ 2)$$

Using these relations in (10.2), we get

$$
\begin{aligned}
&\ddot{U}_1 + \gamma_1 \frac{\dot{U}_1 + \varepsilon\dot{W}_1}{1+\varepsilon} + \frac{U_1 + \varepsilon W_1}{1+\varepsilon} + \gamma_{12}\frac{\dot{U}_1 + \varepsilon\dot{W}_1}{1+\varepsilon} + \alpha_{12}\frac{U_1 + \varepsilon W_1}{1+\varepsilon} + \\
&\quad - \gamma_{12}\frac{\dot{U}_2 + \varepsilon\dot{W}_2}{1+\varepsilon} - \alpha_{12}\frac{U_2 + \varepsilon W_2}{1+\varepsilon} = f_{10}\sin(\Omega_1\tau) \\
&\ddot{W}_1 + \gamma_1 \frac{\dot{U}_1 + \varepsilon\dot{W}_1}{1+\varepsilon} + \frac{U_1 + \varepsilon W_1}{1+\varepsilon} + \gamma_{12}\frac{\dot{U}_1 + \varepsilon\dot{W}_1}{1+\varepsilon} + \alpha_{12}\frac{U_1 + \varepsilon W_1}{1+\varepsilon} + \\
&\quad - \gamma_{12}\frac{\dot{U}_2 + \varepsilon\dot{W}_2}{1+\varepsilon} - \alpha_{12}\frac{U_2 + \varepsilon W_2}{1+\varepsilon} = \\
&\quad = -(1+\kappa)\sum_j \dot{W}_1^-\delta(\tau - \tau_j) + f_{20}\sin(\Omega_2\tau) \\
&\ddot{U}_2 + \gamma_2 \frac{\dot{U}_2 + \varepsilon\dot{W}_2}{1+\varepsilon} + \Omega_{20}^2\frac{U_2 + \varepsilon W_2}{1+\varepsilon} + \gamma_{12}\frac{\dot{U}_2 + \varepsilon\dot{W}_2}{1+\varepsilon} + \alpha_{12}\frac{U_2 + \varepsilon W_2}{1+\varepsilon} + \\
&\quad - \gamma_{12}\frac{\dot{U}_1 + \varepsilon\dot{W}_1}{1+\varepsilon} - \alpha_{12}\frac{U_1 + \varepsilon W_1}{1+\varepsilon} = f_{20}\sin(\Omega_2\tau) \\
&\ddot{W}_2 + \gamma_2 \frac{\dot{U}_2 + \varepsilon\dot{W}_2}{1+\varepsilon} + \Omega_{20}^2\frac{U_2 + \varepsilon W_2}{1+\varepsilon} + \gamma_{12}\frac{\dot{U}_2 + \varepsilon\dot{W}_2}{1+\varepsilon} + \alpha_{12}\frac{U_2 + \varepsilon W_2}{1+\varepsilon} + \\
&\quad - \gamma_{12}\frac{\dot{U}_1 + \varepsilon\dot{W}_1}{1+\varepsilon} - \alpha_{12}\frac{U_1 + \varepsilon W_1}{1+\varepsilon} = \\
&\quad = -(1+\kappa)\sum_j \dot{W}_2^-\delta(\tau - \tau_j) + f_{20}\sin(\Omega_2\tau)
\end{aligned}
\tag{10.3}
$$

As can be seen, the left-hand sides of all the equations are more complicated now. However, the impact-related sums are present only in the differential equations corresponding to variables W_i.

10.3 Analytical Treatment of the Problem

In the approximate analytical approach to the problem, the mass ratio plays a role of the small parameter ($\varepsilon \ll 1$). From the physical viewpoint, some factors within the system are assumed to be weak, and the following parameters are formally introduced:

$$\gamma_i = \varepsilon\hat{\gamma}_i, \quad \alpha_{12} = \varepsilon\hat{\alpha}_{12}, \quad \gamma_{12} = \varepsilon\hat{\gamma}_{12}, \quad f_{i0} = \varepsilon\hat{f}_{i0}. \tag{10.4}$$

Moreover, we focus on the most common type of motion studied in the field of vibro-impact systems, i.e. periodic oscillations with two impacts per cycle, near 1:1 resonance. Let us describe the proximity of Ω_{20} and Ω_1, Ω_2 to the natural frequency (normalized to unity) of the first LO by

$$\Omega_{20}^2 = 1 + \sigma_{20}, \quad \Omega_1 = \Omega_2 = 1 + \sigma_e, \tag{10.5}$$

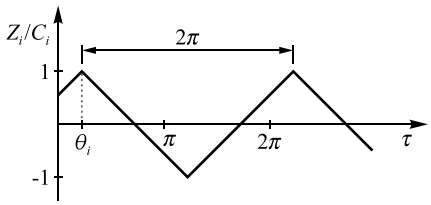

Fig. 10.3 The saw-tooth function used as a part of the solution W_{i0}

where the detuning parameters can be expressed as

$$\sigma_{20} = \varepsilon\hat{\sigma}_{20}, \quad \sigma_e = \varepsilon\hat{\sigma}_e. \tag{10.6}$$

In the following analysis, the method of multiple scales is employed [1, 2]. Two time scales are used:

$$\tau_k = \varepsilon^k \tau, \qquad k = 0,\ 1$$

and the solution of the problem is approximated by

$$U_i = U_{i0}(\tau_0,\ \tau_1) + \varepsilon U_{i1}(\tau_0,\ \tau_1), \qquad W_i = W_{i0}(\tau_0,\ \tau_1) + \varepsilon W_{i1}(\tau_0,\ \tau_1). \tag{10.7}$$

Substituting expansions (10.7), frequencies (10.5) with (10.6), and parameters (10.4) into (10.3), and then equating coefficients of order ε^0, we obtain

$$\begin{aligned} &D_0^2 U_{i0} + U_{i0} = 0, \\ &D_0^2 W_{i0} = -(1+\kappa)\sum_j D_0 W_{i0}^- \delta(\tau_0 - \tau_{0j}) - U_{i0}, \end{aligned} \tag{10.8}$$

where $D_k^n = \partial^n / \partial \tau_k^n$. For the first equation, the solution is simply

$$U_{i0} = B_i(\tau_1)\sin(\tau_0 + \phi_i(\tau_1)). \tag{10.9}$$

In the second case, in turn, we assume that

$$W_{i0} = B_i(\tau_1)\sin(\tau_0 + \phi_i(\tau_1)) + Z_i(\tau_0,\ \tau_1), \tag{10.10}$$

where Z_i is the saw-tooth function

$$Z_i(\tau_0,\ \tau_1) = \frac{2}{\pi} C_i(\tau_1)\arcsin[\cos(\tau_0 - \theta_i(\tau_1))] \tag{10.11}$$

which describes the non-smooth nature of the motion due to impacts that occur at $\tau_{0j} = j\pi + \theta_i$ for $j = 0,\ 1,\ 2,\ \ldots$. This specific part of the solution for constant C_i and θ_i is presented graphically in Fig. 10.3.

In order to determine relations between B_i and C_i, we analyze the impact conditions. Firstly, it is assumed that $W_i = \pm 1$ for $\tau_{0j} = j\pi + \theta_i$. Taking into account (10.10), we get

$$B_i \sin(\theta_i + \phi_i) + C_i = 1 \tag{10.12}$$

Secondly, inserting solution (10.10) to the second equation of (10.8) leads to

$$\frac{\partial^2 Z_i}{\partial \tau_0^2} + (1+\kappa) \sum_j \left[B_i \cos(\tau_0 + \phi_i) + \frac{\partial Z_i^-}{\partial \tau_0} \right] \delta(\tau_0 - \tau_{0j}) = 0. \tag{10.13}$$

After integration of this equation over a small time interval around $\tau_0 = \theta_i$, we obtain:

$$-\frac{4}{\pi} C_i + (1+\kappa) \left[B_i \cos(\theta_i + \phi_i) + \frac{2}{\pi} C_i \right] = 0. \tag{10.14}$$

A combination of (10.12) and (10.14) gives the following relation between the slow-time-scale variables:

$$C_i = \frac{1 \pm \sqrt{(1+\rho^2) B_i^2 - \rho^2}}{1+\rho^2}, \qquad \rho = \frac{2(1-\kappa)}{\pi(1+\kappa)} \tag{10.15}$$

or alternatively

$$B_i^2 = 1 - 2C_i + (1+\rho^2) C_i^2. \tag{10.16}$$

The equations define the so called slow invariant manifold (SIM) of the problem for the case of 1:1 resonance. Furthermore, the phase angles, ϕ_i and θ_i, are specified by the formulas:

$$\sin(\theta_i + \phi_i) = \frac{1 - C_i}{B_i}, \qquad \cos(\theta_i + \phi_i) = \frac{\rho C_i}{B_i}. \tag{10.17}$$

In order to find the fixed points and observe the evolution of the system on the SIM, the equations related to U_i at the higher order of approximation (ε^1) are used (due to their complexity they are not presented in the full form):

$$\begin{aligned} D_0^2 U_{11} + U_{11} &= g_1(\tau_0,\ U_{10},\ W_{10},\ U_{20}), \\ D_0^2 U_{21} + U_{21} &= g_2(\tau_0,\ U_{20},\ W_{20},\ U_{10}). \end{aligned} \tag{10.18}$$

The functions Z_i included on the right hand sides, g_i, can be expanded into a Fourier series (with respect to τ_0):

$$Z_i = \frac{8}{\pi^2} C_i \sum_{n=1,3,5}^{\infty} \frac{1}{n^2} \cos[n(\tau_0 - \theta_i)] \tag{10.19}$$

Next, elimination of secular terms provides the solvability conditions, i.e. the system of differential equations for the amplitudes and phases:

$$\begin{aligned} D_1 B_1 &= h_{B1}(\tau_1,\ B_1,\ \phi_1,\ B_2,\ \phi_2,\ C_1,\ \theta_1),\\ D_1 \phi_1 &= h_{\phi 1}(\tau_1,\ B_1,\ \phi_1,\ B_2,\ \phi_2,\ C_1,\ \theta_1),\\ D_1 B_2 &= h_{B2}(\tau_1,\ B_1,\ \phi_1,\ B_2,\ \phi_2,\ C_2,\ \theta_2),\\ D_1 \phi_2 &= h_{\phi 2}(\tau_1,\ B_1,\ \phi_1,\ B_2,\ \phi_2,\ C_2,\ \theta_2). \end{aligned} \tag{10.20}$$

To transform (10.20) into an autonomous system, we use relations (10.17) and put

$$\psi_1 = \hat{\sigma}_e \tau_1 - \phi_1, \qquad \psi_2 = \hat{\sigma}_e \tau_1 - \phi_2. \tag{10.21}$$

Consequently, we obtain

$$\begin{aligned} D_1 B_1 &= h^*_{B1}(B_1,\ \psi_1,\ B_2,\ \psi_2,\ C_1),\\ D_1 \psi_1 &= h^*_{\psi 1}(B_1,\ \psi_1,\ B_2,\ \psi_2,\ C_1),\\ D_1 B_2 &= h^*_{B2}(B_1,\ \psi_1,\ B_2,\ \psi_2,\ C_2),\\ D_1 \psi_2 &= h^*_{\psi 2}(B_1,\ \psi_1,\ B_2,\ \psi_2,\ C_2). \end{aligned} \tag{10.22}$$

The steady-state motions correspond to the solutions of the algebraic system

$$h^*_{B1} = 0, \qquad h^*_{\psi 1} = 0, \qquad h^*_{B2} = 0, \qquad h^*_{\psi 2} = 0. \tag{10.23}$$

Finally, determining $\sin\psi_i$, $\cos\psi_i$ and $\sin(\psi_2 - \psi_1)$, $\cos(\psi_2 - \psi_1)$ appearing in (10.23), and using elementary trigonometric identities, we can eliminate ψ_i and arrive at the rational equations in which B_i, C_i are the only unknowns:

$$h_1(B_1,\ C_1,\ B_2,\ C_2) = 0, \qquad h_2(B_1,\ C_1,\ B_2,\ C_2) = 0. \tag{10.24}$$

Solving these equations together with (10.16), we can find the fixed points of the slow flow.

The SIM, that is the curve $B_i(C_i)$, is shown in Fig. 10.4. The minimal allowable (real) value of B_i and the corresponding value of C_i are given by

$$B_{\min} = \frac{\rho}{\sqrt{1+\rho^2}}, \qquad C_{\min} = \frac{1}{1+\rho^2} \tag{10.25}$$

A careful analysis of the function $W_{i0}(\tau_0,\ \tau_1)$ leads to the conclusion that non-degenerate solutions, i.e. the ones that do not violate the no-penetration condition ($|W_{i0}| \leqslant 1$ for all τ_0), exist for $C_i \geq 0$.

Moreover, the curve $B_i(C_i)$ can be divided into two branches: one is stable and the other is unstable. Stability of periodic motions can be studied by means of the technique proposed by Masri [16] and adopted, for example, in [17, 18]. The approach

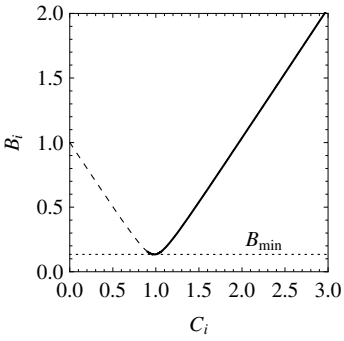

Fig. 10.4 SIM of the system for $\kappa = 0.65$: the stable branch (bold solid) and the unstable branch (dashed); dotted line depicts the $B_{\min}$ level

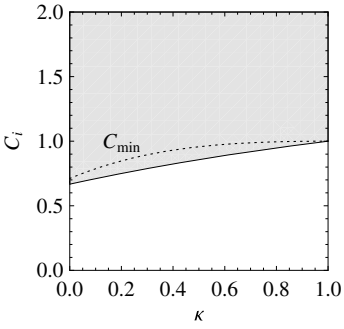

Fig. 10.5 Stable (shaded) and unstable (white) regions for the vibro-impact system; dotted line depicts the $C_{\min}(\kappa)$ curve

allows one to analyze the propagation of small perturbations in the original periodic motion. More precisely, one can evaluate the effect of small variation of the steady-state values (displacement and velocity) just after an impact, $(\Delta_1\theta_i^+,\ \Delta_1\dot{W}_i^+)$, on the instants of subsequent collisions and the resulting variation in the displacement and velocity, i.e. $(\Delta_j\theta_i^+,\ \Delta_j\dot{W}_i^+)$ with $j = 2,\ 3,\ \ldots$. More detailed discussion of the technique goes beyond the scope of this paper. Such an analysis conducted for the considered system leads to the following condition for the existence of asymptotically stable periodic motions:

$$C_i > \frac{4}{4+\pi\rho}. \tag{10.26}$$

The stability region on the plane $(\kappa,\ C_i)$ is presented in Fig. 10.5. As can be seen, the right arm $(C_i > C_{\min})$ of the hyperbola $B_i(C_i)$ belongs entirely to the stable branch, which additionally contains a short piece of the left arm $(C_i < C_{\min})$.

10.4 Analytical-Numerical Results

The results presented below have an analytical-numerical character. Firstly, due to the complexity of the system of algebraic equations (10.16)–(10.24), the fixed points of

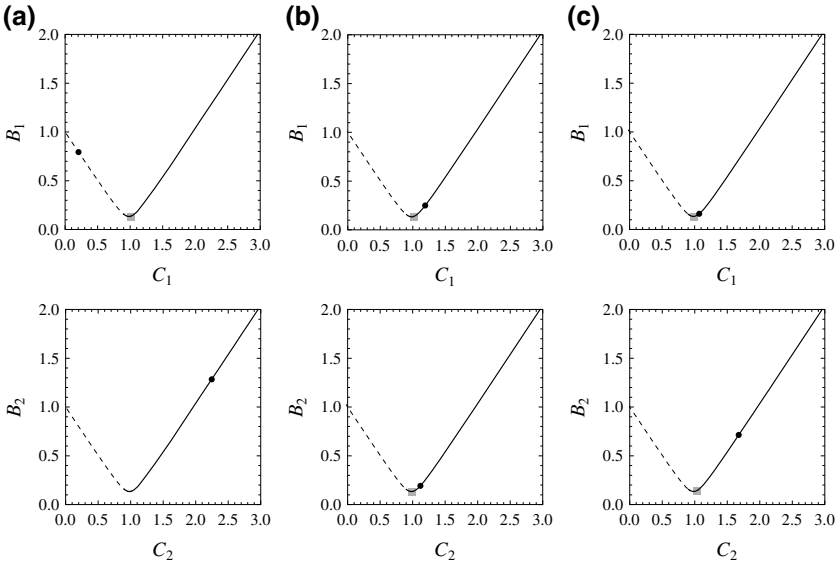

Fig. 10.6 Fixed points of the system: **a** unstable, **b** stable, **c** stable. Results obtained for $\hat{f}_{10} = \hat{f}_{20} = 1$

the slow flow are searched numerically. Secondly, the theoretically predicted steady-state responses of the system are compared to the purely numerical solutions, i.e. the results obtained by a direct numerical integration of (10.1). All the numerical experiments are performed for the following set of dimensionless parameters:

$$\varepsilon = 0.1, \qquad \kappa = 0.65, \qquad \hat{\alpha}_{12} = 1,$$
$$\hat{\gamma}_1 = \hat{\gamma}_2 = \hat{\gamma}_{12} = 0.2, \qquad \hat{\sigma}_{20} = 0.5, \qquad \hat{\sigma}_e = 0.2.$$

Values of the excitation amplitudes will be altered.

Let us start with identical amplitudes of two forces: $\hat{f}_{10} = \hat{f}_{20} = 1$. Three fixed points existing in this case are illustrated in Fig. 10.6. More precisely, the projection of the fixed points on the $(C_i,\ B_i)$ planes are represented by black circles. The projection on the $(C_1,\ B_1)$ plane located on the left arm of the SIM (see Fig. 10.6a) indicates that the corresponding fixed point is unstable; the next two ones are stable.

The theoretically predicted steady-state response of the system (two impacts per cycle) for the stable fixed point (c) is presented in Fig. 10.7. The absolute displacements of the primary oscillators and the coordinates U_i are marked in grey while the absolute and relative displacements of the particles are shown in black lines. Similar results can be obtained numerically. Needless to say, in a dynamic simulation, a long-term behaviour of the system must be analyzed to omit any transient motion. As an example, the purely numerical solutions W_2 and X_2 are given in Fig. 10.8.

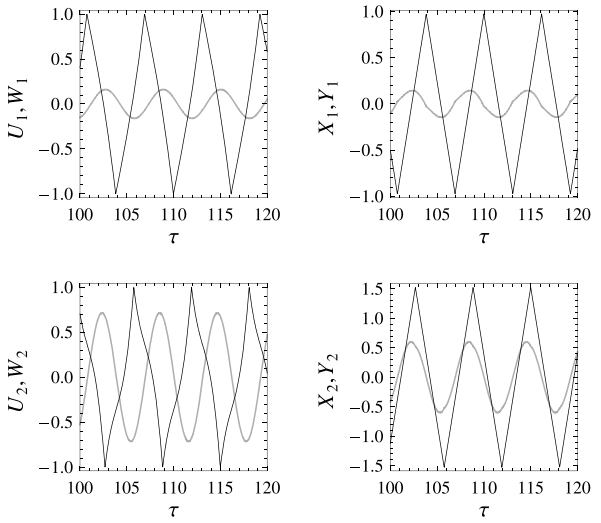

Fig. 10.7 Steady-state response of the system – fixed point (c): U_i, X_i (grey) and W_i, Y_i (black). Results obtained for $\hat{f}_{10} = \hat{f}_{20} = 1$

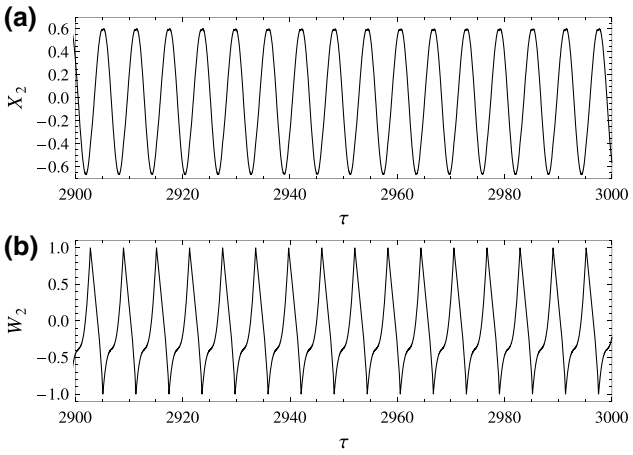

Fig. 10.8 Steady-state response of the system: **a** displacement of the second box, **b** relative displacement of the particle. Numerical solution obtained for $\hat{f}_{10} = \hat{f}_{20} = 1$

The grey squares appearing in Fig. 10.6 are related to singular points. Let $P_1 = (C_1^*,\ B_1^*)$ and $P_2 = (C_2^*,\ B_2^*)$ be the projections of a fixed point onto $(C_1,\ B_1)$ and $(C_2,\ B_2)$ planes, respectively. By S_1 we denote a point on $(C_1,\ B_1)$ corresponding to a singularity of h_1 and h_2 in (10.24) at $C_2 = C_2^*$ and $B_2 = B_2^*$. Analogously, S_2 on the $(C_2,\ B_2)$ plane comes from a singularity of h_1 and h_2 when $C_1 = C_1^*$ and $B_1 = B_1^*$. Obviously, locations of P_1, P_2 and S_1, S_2 on the SIM projections change

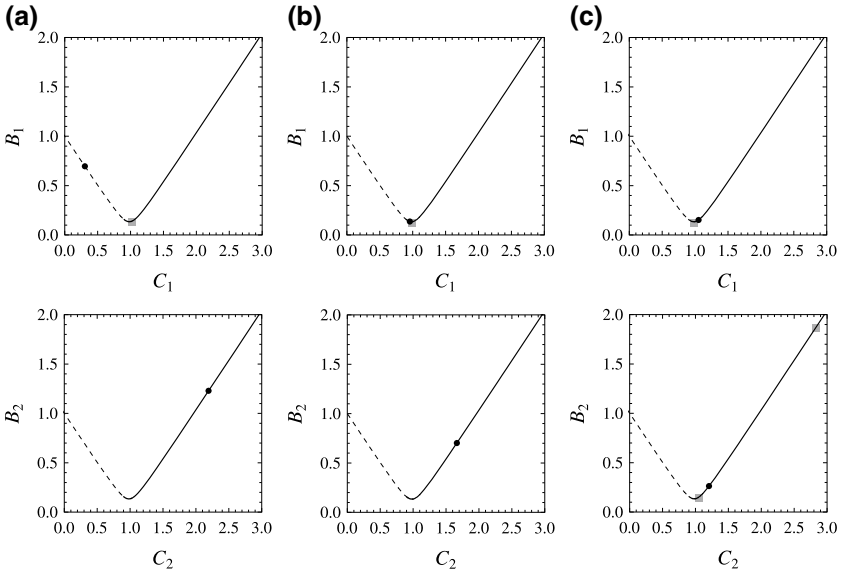

Fig. 10.9 Fixed points of the system: **a** unstable, **b** unstable, **c** stable. Results obtained for $\hat{f}_{10} = 1$, $\hat{f}_{20} = 0.89$

with varying values of some parameters. However, if P_i gets closer to S_i, the fixed point becomes a singular point, potentially associated to a bifurcation.

Now, let us decrease one of the excitation amplitudes. For $\hat{f}_{20} = 0.89$, there are still three fixed points (see Fig. 10.9), but only one of them turns out to be stable. As can be seen from a comparison of all cases in Figs. 10.6 and 10.9, the projections P_1 and P_2 move along the SIM-related curves from right to left. Particularly, projections of the stable fixed points move down the right branch of the SIM.

As the last example, let us consider the case when both the excitation amplitudes are decreased up to 0.5. In such a case only one fixed point exists. Its projections on the $(C_i,\ B_i)$ planes as well as the corresponding steady-state response are presented in Fig. 10.10. However, since P_1 and P_2 are located on the left branch of the SIM, the fixed point is unstable. The only possible behaviour for the system is the so called strongly modulated response (SMR). Thus, the analytical periodic solution has no practical importance. The actual motion of the system can be observed by means of numerical simulations. As can be seen from Fig. 10.11, in the relative displacement of a particle we can distinguish intervals of resonant motion divided by relatively short, irregular non-resonant behaviour. The primary oscillators, in turn, undergoe the characteristic beating-like motion, i.e. large modulations of the vibration amplitudes.

To sum up, when treating the forces amplitudes as the control parameters, we can observe a series of changes in the location of fixed points on the SIM and their stability. By decreasing the amplitudes, we can lead to the case when no stable fixed points exist, and the mechanical system exhibits strongly modulated response that

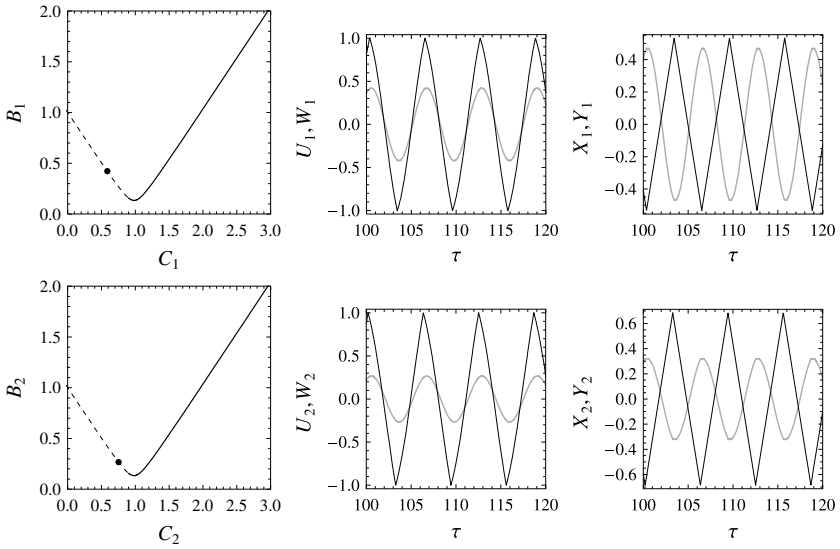

Fig. 10.10 Fixed point (unstable) and the theoretical response of the system: U_i, X_i (grey) and W_i, Y_i (black). Results obtained for $\hat{f}_{10} = \hat{f}_{20} = 0.5$

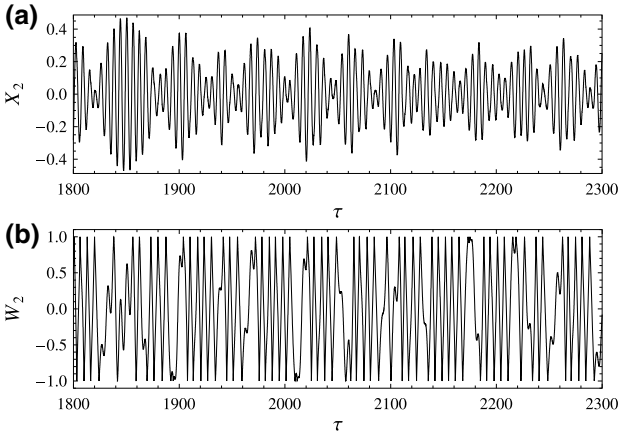

Fig. 10.11 Strongly modulated response of the system: **a** displacement of the second box, **b** relative displacement of the particle. Numerical solution obtained for $\hat{f}_{10} = \hat{f}_{20} = 0.5$

may be advantageous for potential energy harvesting applications [8, 13]. Analysis of the interplay between various model parameters goes beyond the scope of this paper.

10.5 Conclusions

The four-degree-of-freedom system composed of two weakly coupled vibro-impact modules under harmonic forces has been considered. The analytical approach based on the multiple scales method combined with the saw-tooth impact modelling has been adopted and used. The response of the system with two impacts per cycle near 1:1 resonance has been studied.

The applied technique can provide semi-analytical periodic solutions, and is useful in assessing stability of the solutions. It should be noticed that this approach does not require the restitution coefficient to be close to unity. Validity of the analytical predictions has been examined by numerical experiments.

Naturally, such a mechanical system can undergo complex behaviours, and many interesting problems may be studied in detail, e.g. stability of fixed points, singular points and bifurcations, interplay between different model parameters. Apart from that, the applicability of the method to more complex mechanical systems should be verified and extended. Particularly, models including strong and nonlinear couplings, and one-sided impact interactions merit further attention.

References

1. V. Marinca, N. Herisanu, *Nonlinear Dynamical Systems in Engineering: Some Approximate Approaches* (Springer, Heidelberg, 2011)
2. A.H. Nayfeh, D.T. Mook, *Nonlinear Oscillations* (Wiley, New York, 1995)
3. R. Ibrahim, *Vibro-Impact Dynamics: Modeling, Mapping and Applications* (Springer, Berlin, 2009)
4. V. Pilipchuk, Analytical study of vibrating systems with strong non-linearities by employing saw-tooth time transformations. J. Sound Vib. **192**, 43–64 (1996)
5. V. Pilipchuk, A. Vakakis, M. Azeez, Study of a class of subharmonic motions using a non-smooth temporal transformation (NSTT). Phys. D **100**, 145–164 (1997)
6. V. Pilipchuk, Impact modes in discrete vibrating systems with rigid barriers. Int. J. Nonlinear Mech. **36**, 999–1012 (2001)
7. O. Gendelman, Analytic treatment of a system with a vibro-impact nonlinear energy sink. J. Sound. Vib. **331**, 4599–4608 (2012)
8. O. Gendelman, A. Alloni, Forced system with vibro-impact energy sink: chaotic strongly modulated responses. Procedia IUTAM **19**, 53–64 (2016)
9. T. Li, S. Seguy, A. Berlioz, Dynamics of cubic and vibro-impact nonlinear energy sink: analytical, numerical, and experimental analysis. J. Vib. Acoust. **138**, 031010 (2016)
10. T. Li, S. Seguy, A. Berlioz, Optimization mechanism of targeted energy transfer with vibro-impact energy sink under periodic and transient excitation. Nonlinear Dyn. **87**, 2415–2433 (2016)

11. T. Li, S. Seguy, A. Berlioz, On the dynamics around targeted energy transfer for vibro-impact nonlinear energy sink. Nonlinear Dyn. **87**, 1453–1466 (2017)
12. T. Li, D. Qiu, S. Seguy, A. Berlioz, Activation characteristic of a vibro-impact energy sink and its application to chatter control in turning. J. Sound Vib. **405**, 1–18 (2017)
13. A. Vakakis, O. Gendelman, L. Bergman, D. McFarland, G. Kerschen, Y. Lee, *Nonlinear Targeted Energy Transfer in Mechanical and Structural Systems*. Solid Mechanics and Its Applications (Springer, 2009)
14. V. Babitsky, *Theory of Vibro-Impact Systems and Applications* (Springer, Berlin, 1998)
15. S. Thornton, J. Marion, *Classical Dynamics of Particles and Systems* (Brooks/Cole, Belmont, 2004)
16. S. Masri, Analytical and experimental studies of impact dampers. Ph.D. thesis, California Institute of Technology (1965)
17. K. Czolczynski, B. Blazejczyk-Okolewska, A. Okolewski, Analytical and numerical investigations of stable periodic solutions of the impacting oscillator with a moving base. Int. J. Mech. Sci. **115–116**, 325–338 (2016)
18. N. Popplewell, C. Bapat, K. McLachlan, Stable periodic vibroimpacts of an oscillator. J. Sound Vib. **87**, 41–59 (1983)